

AEROELASTIC DYNAMICAL RESPONSE AND CONTROL OF AN AIRFOIL SECTION WITH SHAPE MEMORY ALLOY (SMA)

Vinícius Piccirillo, pcmec@ita.br

Luiz Carlos Sandoval Góes, goes@ita.br

Department of Engineering Aeronautical and Mechanical, Technological Institute of Aeronautics – ITA, 12228 – 900, Sao Jose dos Campos, SP, Brazil

José Manoel Balthazar, jmbaltha@rc.unesp.br

Department of Statistic, Applied Mathematical and Computation, Sao Paulo State University – UNESP, 13500 – 230, Rio Claro, SP, Brazil

Abstract. *This paper concerns the active aeroelastic control of wing-flap systems operating in an incompressible flow field. The goal is to implement actuators utilizing the shape memory alloy for active flap control capability to suppress the flutter instability. Based on the state-dependent Riccati equation method, a state feedback suboptimal control law is found for control current applied in the system, controlling thus the temperature in the SMA actuator. The simulation results show that the SMA nonlinear actuator leads to an better response in closed-loop system.*

Keywords: *Aeroelasticity, Shape Memory Alloy, Airfoil Motions, Optimal control*

NOMENCLATURE

a	Nondimensionalized distance from the mid-chord to the elastic axis	L	Aerodynamic lift force
A_S	Austenite start temperature	m	Mass of airfoil per unit span
A_f	Austenite final temperature	M_α	Aerodynamic pitching moment about elastic axis
b	Semi-chord of the wing	M_S	Martensite start temperature
D	Elastic modulus of the SMA material	M_f	Martensite final temperature
D_A	Austenite Elastic modulus	T	SMA wire's temperature
D_M	Martensite Elastic modulus	V	Free stream velocity
h	Plunge displacement	δ	SMA wire's martensite faction factor
I_α	Mass moment of inertia of the wing about the elastic axis	ε_R	Maximum residual strain
I_β	Mass moment of inertia of the aileron about aileron hinge	ρ	Air density
J_T	Inertia moment of hinge tube	σ	SMA wire's stress
K_h	Structural spring constant in plunge	ϕ	Wagner's function
K_α	Structural spring constant in pitch	Θ	SMA wire's thermal expansion factor
		Ω	Phase transformation contribution factor

1. INTRODUCTION

Aeroelasticity is the dynamic interaction of structural, inertial, and aerodynamic forces. Conventional methods of examining aeroelastic behavior have relied on a linear approximation of the governing equations which describe both the flow field and the structure, Dowell et al. (2008). Mukhopadhyay (2003) presented a historical perspective on analysis and control of aeroelastic responses. In recent years, a large number of control strategies have been developed for the flutter suppression, such as adaptive decoupled fuzzy sliding-mode control, Lin and Chin, (2006), SDRE control technique was developed to design suboptimal control laws for nonlinear aeroelastic systems, Tadi (2003), and Gain scheduled controllers have been designed, Barker and Balas, (2000).

Flaps are hinged surfaces on the trailing edge of the wings of a fixed-wing aircraft. As flaps are extended, the stalling speed of the aircraft is reduced, which means that the aircraft can fly safely at slower speeds (especially during take off and landing). Extending flaps increases the camber of the wing airfoil, thus raising the maximum lift coefficient. This increase in lift coefficient allows the aircraft to generate a given amount of lift for a slower speed. Therefore, extending the flaps reduces the stalling speed of the aircraft.

Shape memory alloys (SMAs) refer to a materials group which has the ability to return to a predetermined shape when heated. The source of the distinctive mechanical behavior of these materials is a crystalline phase transformation between a high symmetry (austenite), and a low symmetry (martensite).

The SMAs present high reversible strains compared to the conventional materials (pseudoelastic effect) and permanent deformations that disappear upon an increase in temperature (shape memory effect (SME)). In the shape memory effect, an SMA material exhibits a large residual strain after the loading and unloading. This strain can be fully recovered upon heating the material. In the pseudoelastic effect, the SMA material achieves a very large strain upon loading, which is fully recovered in a hysteresis loop upon unloading. The observable macroscopic mechanical behavior of SMAs can be separated into two categories: the shape memory effect (Fig. 1a) and pseudoelastic effect (Fig. 1b).

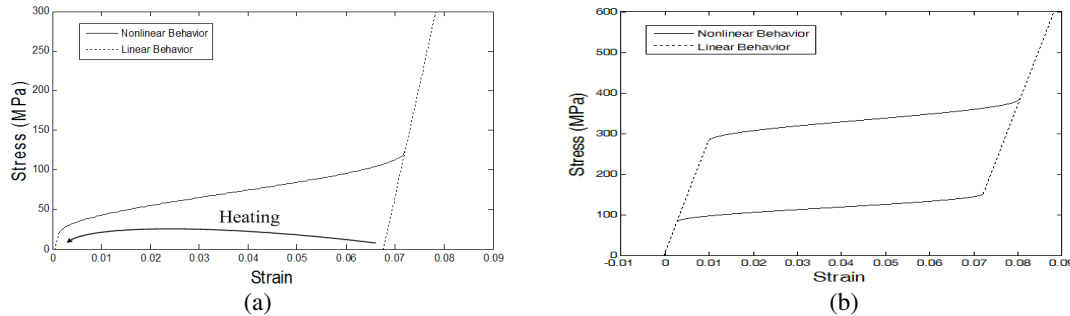


Figure 1: a) Shape memory effect (SME) and b) Pseudoelastic effect

Tawfik et al. (2002) proposed a novel concept in enhancing the thermal buckling and aeroelastic behavior of plates through embedding SMA fibers in it. Gou et al. (2007) investigated the large amplitude nonlinear flutter of thin SMA hybrid composite plates at an arbitrary yaw angle and an elevated temperature. Ibrahim et al. (2008) investigated the nonlinear random response of thick composite plates impregnated with pre-strained shape memory alloy fibers under combined thermal and random acoustic loads.

This work presents a investigating of how use the SMA wire nonlinear actuators to control the flap movement of a typical section. Two SMA nonlinear actuators are used to control the flap movement. One moving the flap down, after of an electrical heating while the another actuator remain at constant temperature. When heated, the wire actuator at the down part contract due to the SME, recovering a portion of their pre-strain and developing a constraining force. The actuation of a trailing-edge is achieved using the shape memory effect. The shape memory effect involves plastically deformation a segment of SMA and then recovering the prescribed pre-strain during phase transformation via heat activation. The Fig. 2 shows the wing section. In Fig. 2a is presented the conventional airfoil with surface control where the elements of this structure are linear. On the other hand, the Fig. 2b shows the system with airfoil-control surface-nonlinear SMA actuator.

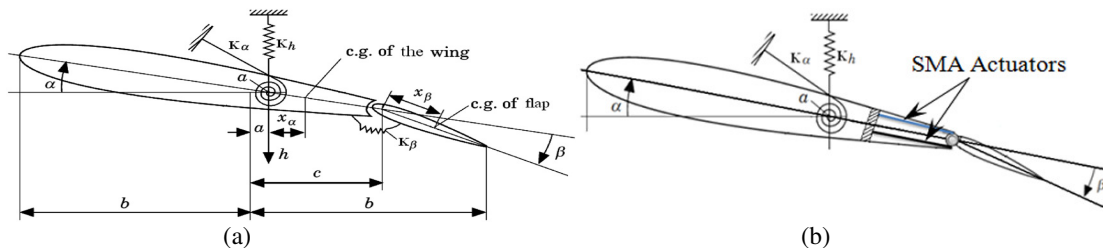


Figure 2: (a) Schematic of airfoil section with a control surface and (b) system airfoil-control surface-SMA actuator

2. SMA CONSTITUTIVE MODELING

An SMA material exists in a completely austenite or martensite phase or fractions of austenite and martensite phases depending on the temperature and stress. A one-dimensional constitutive model was proposed by Brinson (1993) to describe the thermomechanical behavior of SMA. The model uses an internal variable approach to derive a comprehensive constitutive law for SMA materials from first principles without the assumption of constant material functions. The major contribution of the model is the separation of the martensite fraction internal variable into temperature induced and stress induced parts, which allow the derived constitutive law to quite accurately present both the pseudoelastic and shape memory effect at all temperatures.

The motivation for using Brinson model is the flexibility to model the SMA nonlinear behavior closer to reality. The basic equation for the change in stress in the model developed by Brinson (1993) is given by

$$d\sigma = \frac{\partial \sigma}{\partial \epsilon} d\epsilon + \frac{\partial \sigma}{\partial T} dT + \frac{\partial \sigma}{\partial \delta} d\delta \Rightarrow d\sigma = D(\epsilon, \delta, T) d\epsilon + \Theta(\epsilon, \delta, T) dT + \Omega(\epsilon, \delta, T) d\delta \quad (1)$$

If the material functions are assumed to be constants, Equation 1 can be expressed as:

$$\dot{\sigma} = D \dot{\epsilon} + \Theta \dot{T} + \Omega \dot{\delta} \quad (2)$$

where

$$D = D_A + \delta(D_M - D_A), \quad \Omega = -\epsilon_R D \quad (3)$$

Based on the micro-mechanics of the SMA material, Brinson (1993) expressed the Martensite function δ as:

$$\delta = \delta_T + \delta_S \quad (4)$$

where δ_T represents the fraction of the material that is purely temperature induced martensite with multiple variants, and δ_S denotes the fraction of the material that has been transformed by stress into a single martensitic variant. A brief description of the Brinson's constitutive model is given below. Conversion to Martensite - for $T > M_S$ and $\sigma_S^{\text{crit}} + C_M(T - M_s) < \sigma < \sigma_f^{\text{crit}} + C_M(T - M_S)$

$$\delta_S = \frac{1 - \delta_{S_0}}{2} \cos \left\{ \frac{\pi}{\sigma_S^{\text{crit}} - \sigma_f^{\text{crit}}} \left[\sigma - \sigma_f^{\text{crit}} - C_M(T - M_s) \right] \right\} + \frac{1 - \delta_{S_0}}{2}, \quad \delta_T = \delta_{T0} - \frac{\delta_{T0}}{1 - \delta_{S0}} (\delta_S - \delta_{S_0}) \quad (5)$$

when $T < M_S$ and $\sigma_S^{\text{crit}} < \sigma < \sigma_f^{\text{crit}}$

$$\delta_S = \frac{1 - \delta_{S_0}}{2} \cos \left[\frac{\pi}{\sigma_S^{\text{crit}} - \sigma_f^{\text{crit}}} (\sigma - \sigma_f^{\text{crit}}) \right] + \frac{1 - \delta_{S_0}}{2}, \quad \delta_T = \delta_{T0} - \frac{\delta_{T0}}{1 - \delta_{S0}} (\delta_S - \delta_{S_0}) + \Delta_T \quad (6)$$

when $M_f < T < M_S$ and $T < T_0$ we have that $\Delta_T = \frac{1 - \delta_{T0}}{2} \left\{ \cos \left[a_M(T - M_f) \right] + 1 \right\}$, otherwise $\Delta_T = 0$. Conversion to Austenite - $T > A_S$ and $C_A(T - A_f) < \sigma < C_A(T - A_S)$

$$\delta_S = \frac{\delta_{S_0}}{2} \left\{ \cos \left[a_A \left(T - A_s - \frac{\sigma}{C_A} \right) \right] + 1 \right\}, \quad \delta_T = \delta_{T0} \left\{ \cos \left[a_A \left(T - A_s - \frac{\sigma}{C_A} \right) \right] + 1 \right\} \quad (7)$$

3. ACTUATOR CONCEPT

Conventionally, the flaps are controlled via electric motors or hydraulic actuators. Actuators made of shape memory alloy (SMA) have the advantage of higher power-to-weight ratio as compared to conventional electric or hydraulic actuators, Mavroidis (2002). Figure 3 show a typical section with two SMA wire actuators. In the figure, an upper and a lower of SMA wires, are fixed at one end and connected to a hinge tube at the other end, and the wire are used to actuate a flap. Both wires are assumed to have the same initial length l_{wire} , the same plastic deformation ϵ_0 , and cross section area A_R . Considering that the upper and lower parts of the wire are thermally and electrically isolated from each other and are heated by resistivity.

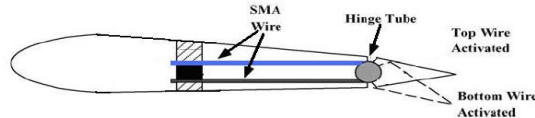


Figure 3: Diagram configuration of the typical section using the SMA wire actuator

The flap deflection concept is described in Fig. 4. Here, both SMA wires are in the transformed state of the 50% martensite phase under residual stress. The residual stress state is generated by the interaction between two SMA wires. To flap deflection downward, the lower wires are heated while the upper wires remain at constant temperature. When heated, the lower wires contract due to the SME, recovering a portion of their pre-strain and developing a constraining force. The force produces a clockwise moment about the hinge tubes shaft axis, rotating the hinge tube and,

consequently, deflecting the flap downward. The upper wire, at constant temperature, is elongated the same amount that the lower wire. Note that the plastic deformation of the upper wire is increased by the amount that they are elongated. As the wire is elongated, their load-displacement characteristics dictate the amount of force that the system develops.

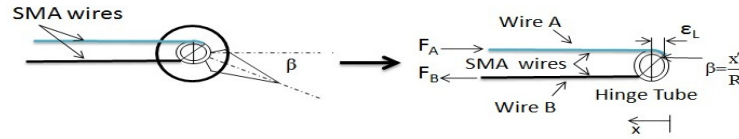


Figure 4: Free body diagram of the SMA wire actuator

The temperature cycle which is induced to the double SMA wires actuator is shown in Fig. 5a. Both SMA wires are transformed into 50% martensite phase initially. First, wire B (black color) is heated from 20 to 90 °C (step 1) and, wire A (blue color) is sustained at 20 °C (step 1). Second, wire B is cooled from 90 to 20 °C while the temperature of wire A is sustained at 20 °C (step 2). A diagram to estimate the forces on the SMA actuator B is shown in Fig. 5b, where the x coordinate represents the position of the actuator. Considered that the Fig. 5b show the behavior of SMA actuator B in their three possible states. In the pure austenite phase, l_0 is considered the length of SMA actuator B. In 50% martensite phase, the SMA actuator B reaches its maximum length l_{wire} , which also corresponds to the situation where the load is in position $x = 0$. The difference between the length l_0 and l_{wire} is approximately 5% of the initial length l_{wire} . An intermediate phase deformation Δl_B in relation to their length l_0 is given by $5\%l_{wire} - x$.

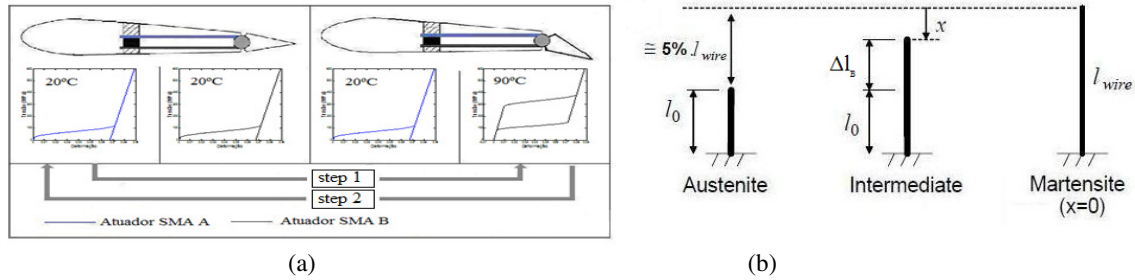


Figure 5: (a) The actuation of the SMA actuator and the current position of each SMA wire along given thermal steps and b) SMA wire behavior actuator B

As the angular velocity of the hinge tube is given by $\beta' = \frac{(L_A - L_B)}{r_T} \Rightarrow \beta' = \frac{x'}{r_T}$, where L_A and L_B is the length of actuator A and B, respectively, therefore, we obtain that $x = \beta r_T$. Thus,

$$\Delta l_B = 0.05l_{fio} - r_T\beta \quad (8)$$

The stress and strain compatibility conditions define the states of the system during actuation. For wire A and wire B these are given as $\Delta l_A = -\Delta l_B$. The forces given by the SMA actuators A and B are represented by F_A and F_B , which can be estimated using the constitutive equations below

$$F_A = \sigma_A A_r \quad (9)$$

$$F_B = \sigma_B A_r \quad (10)$$

4. HEAT TRANSFER MODEL

To simulate the behavior of SMA nonlinear actuators electrically activated the model must be able to describe the contribution of Joule heating to the temperature increase in the actuator. The assumed SMA wire heat transfer equation consists of electrical heating and natural convection, Williams and Elahinia (2008),

$$m_{SMA} C_p \frac{dT}{dt} = I^2 R - hA_R (T - T_\infty) - m_{SMA} \Delta H \dot{\delta} \quad (11)$$

where m_{SMA} is mass per unit length, C_p is the specific heat, R is electrical resistance of the wire, h is the heat convection coefficient, A_R is the circumferential area of the SMA wire. Also, V is the applied voltage, T_∞ is the ambient temperature, ΔH is the latent heat, and $\dot{\delta}$ is the phase transformation rate. Assume also the following cases:

- The temperature is uniform along the length of the wire.
- The room temperature will be constant over time.
- The deformations of the SMA actuator are uniform during the phase transformations.
- Will be considered only the effects of convection and heat conduction.

The electrical resistance of SMA actuators is variable as a result of phase transformation is given by the following equation Elahinia and Ahmadian (2005);

$$R = R_A + \delta(R_M - R_A) \quad (12)$$

the subscripts A and M indicate the austenite and martensite phases, respectively.

5. EQUATION OF MOTION OF THE SYSTEM AIRFOIL-CONTROL SURFACE-SMA ACTUATOR

Defining the actuator behavior now is necessary to make the modeling these actuators. The SMA wire strain rate $\dot{\epsilon}$ and angular velocity $\dot{\beta}$ are related kinematically as

$$\dot{\epsilon} = \left(\frac{r_T}{l_0} \right) \dot{\beta} \quad (13)$$

where r_T is the hinge tube radius and l_0 is the initial length of the SMA wire. For simplicity, in the rest of the text the term airfoil-CS-SMA actuator will be used to describe the system airfoil-control surface-SMA actuator. Thus, the equation of motion that governs the airfoil-CS-SMA actuator may be written as

$$mh'' + mbx_\alpha \alpha'' + mbx_\beta \beta'' + \bar{F}(h) = -L \quad (14)$$

$$mbx_\alpha h'' + I_\alpha \alpha'' + \left((c_\beta - a_h) b^2 mx_\beta + I_\beta \right) \beta'' + M(\alpha) = M_\alpha \quad (15)$$

$$mbx_\beta h'' + \left((c_\beta - a_h) b^2 mx_\beta + I_\beta \right) \alpha'' + (J_T + I_\beta) \beta'' - \sigma^B A (0.05l_{fio} - r_T \beta) + \sigma^A A (0.05l_{fio} + r_T \beta) = M_\beta \quad (16)$$

$$\sigma'^A = D^A \left(\frac{r_T}{l_0} \right) \beta' + \Omega^A \delta'^A + \Theta^A (T^A - T_0^A) \quad (17)$$

$$\sigma'^B = D^B \left(\frac{r_T}{l_0} \right) \beta' + \Omega^B \delta'^B + \Theta^B (T^B - T_0^B) \quad (18)$$

$$\frac{dT^A}{dt} = \frac{I_A^2 R}{m_{SMA} C_p} - \frac{h(T) A_R (T^A - T_\infty)}{m_{SMA} C_p} - \frac{\Delta H \delta'}{C_p} \quad (19)$$

$$\frac{dT^B}{dt} = \frac{I_B^2 R}{m_{SMA} C_p} - \frac{h(T) A_R (T^B - T_\infty)}{m_{SMA} C_p} - \frac{\Delta H \delta'}{C_p} \quad (20)$$

The nondimensional equation of motion of the system airfoil-CS-SMA actuator is given by the following below equation

$$\ddot{\xi} + x_\alpha \ddot{\alpha} + x_\beta \ddot{\beta} + \left(\frac{\Omega_1}{U} \right)^2 \xi = p(\tau, \xi, \alpha, \beta) \quad (21)$$

$$\frac{x_\alpha}{r_\alpha^2} \ddot{\xi} + \ddot{\alpha} + \frac{z_\beta}{r_\alpha^2} \ddot{\beta} + \frac{1}{U^2} \alpha = q(\tau, \xi, \alpha, \beta) \quad (22)$$

$$\frac{x_\beta}{I_\beta^2} \ddot{\xi} + \frac{z_\beta}{I_\beta^2} \ddot{\alpha} + \ddot{\beta} + \left(r_T (\Psi^B + \Psi^A) \right) \beta + 0.05 I_{fio} (\Psi^A - \Psi^B) = r(\tau, \xi, \alpha, \beta) \quad (23)$$

$$\dot{\sigma}^A = D^A \left(\frac{r_T}{l_0} \right) \dot{\beta} + \Omega^A \dot{\delta}^A + \frac{\Theta^A}{U \omega_\alpha} (T^A - T_0^A) \quad (24)$$

$$\dot{\sigma}^B = D^B \left(\frac{r_T}{l_0} \right) \dot{\beta} + \Omega^B \dot{\delta}^B + \frac{\Theta^B}{U \omega_\alpha} (T^B - T_0^B) \quad (25)$$

$$\frac{dT^A}{dt} = \frac{I_A^2 R}{m_{SMA} C_p U \omega_\alpha} - \frac{h(T) A_R (T^A - T_\infty)}{m_{SMA} C_p U \omega_\alpha} - \frac{\Delta H \dot{\delta}}{C_p} \quad (26)$$

$$\frac{dT^B}{dt} = \frac{I_B^2 R}{m_{SMA} C_p U \omega_\alpha} - \frac{h(T) A_R (T^B - T_\infty)}{m_{SMA} C_p U \omega_\alpha} - \frac{\Delta H \dot{\delta}}{C_p} \quad (27)$$

where $\tau = \frac{Ut}{b}$, $\xi = \frac{h}{b}$, $x_\alpha = \frac{S_\alpha}{bm}$, $\omega_\xi^2 = \frac{K_h}{I_\alpha}$, $\omega_\alpha^2 = \frac{K_\alpha}{I_\alpha}$, $r_\alpha^2 = \frac{I_\alpha}{mb^2}$, $\mu = \frac{m}{\rho b^2 \pi}$; $p(\tau, \xi, \alpha, \beta) = -\frac{Lb}{mV^2}$,

$q(\tau, \xi, \alpha, \beta) = \frac{M_\alpha}{mV^2 r_\alpha^2}$, $r(\tau, \xi, \alpha, \beta) = \frac{M_\beta}{mV^2 r_\alpha^2}$; Ω_1 and Ω_2 are uncoupled frequency ratios defined as $\Omega_1 = \frac{\omega_\xi}{\omega_\alpha}$,

$\Omega_2 = \frac{\omega_\beta}{\omega_\alpha}$, the parameters related to actuators are $\Psi^A = \frac{\sigma^A A_r}{mb^2 I_\beta^2}$, $\Psi^B = \frac{\sigma^B A_r}{mb^2 I_\beta^2}$, $r_\beta^2 = \frac{(J_T + I_\beta)}{mb^2}$. For incompressible

inviscid flow the aerodynamic force and moments have been formulated for any arbitrary motion of the airfoil and aileron Alighanbari (2002), giving

$$L(\tau) = \pi \rho b V^2 \left[\xi''(\tau) - a_h \alpha''(\tau) - \frac{T_1}{\pi} \beta''(\tau) + \alpha'(\tau) - \frac{T_4}{\pi} \beta'(\tau) + 2\Pi \right], \quad (28)$$

$$M_\alpha(\tau) = \pi \rho b^2 V^2 \left[a_h \xi''(\tau) - \left(\frac{1}{8} + a_h^2 \right) \alpha''(\tau) + \frac{1}{\pi} \left[T_7 + (c_\beta - a_h) T_1 \right] \beta''(\tau) - a_h \alpha'(\tau) - \frac{1}{\pi} \left[T_1 - T_8 - (c_\beta - a_h) T_4 + \frac{T_{11}}{2} \right] \beta'(\tau) - \frac{1}{\pi} (T_4 + T_{10}) \beta + 2 \left(\frac{1}{2} + a_h \right) \Pi \right] \quad (29)$$

$$M_\beta(\tau) = \pi \rho b^2 V^2 \left[\frac{T_{11}}{\pi} \xi''(\tau) + \frac{1}{\pi} \left[T_7 + (c_\beta - a_h) T_1 \right] \alpha''(\tau) + \frac{T_3}{\pi^2} \beta''(\tau) + \frac{1}{\pi} \left[\frac{\sqrt{(1-c_\beta^2)^3}}{3} + T_1 + \frac{T_4}{2} \right] \alpha'(\tau) + \frac{T_4 T_{11}}{2\pi^2} \beta'(\tau) + \frac{T_4 T_{10} - T_5}{\pi^2} \beta(\tau) - \frac{T_{12}}{\pi} \Pi \right] \quad (30)$$

where

$$\Pi = \left[\xi'(0) - a_h \alpha'(0) + \frac{T_{11}}{2\pi} \beta'(0) + \alpha(0) + \frac{T_{10}}{\pi} \beta(0) \right] \varphi(\tau) + \int_0^\tau \varphi(\tau - \sigma) \left[\xi''(\sigma) + a_h \alpha''(\sigma) + \frac{T_{11}}{2\pi} \beta''(\sigma) + \alpha'(\sigma) + \frac{T_{10}}{\pi} \beta'(\sigma) \right] d\sigma \quad (31)$$

The Theodorsen constants $T_i, i=1,2,\dots,13$, are given in Appendix A. These nonlinear equations of motion have previously been solved numerically using both finite difference and describing function methods, Alighanbari (2002). However, it is not easy to study the dynamical behavior of the system using the equations written in the above form. For instance, fixed-point solutions of the system cannot be easily found and analyzed analytically, or unstable periodic solutions of the system may not be easily obtained. Therefore, it is helpful to transform the equations into a set of

ordinary differential equations. This will also make it possible to use the vast literature and computer codes developed for ODEs in the study of our aeroelastic system. The transformation procedure is outlined below.

The conversion could simply be accomplished if the approximate formula for the Wagner function is considered $\phi(\tau) = 1 - \psi_1 e^{-\varepsilon_1 \tau} - \psi_2 e^{-\varepsilon_2 \tau}$, and the following two auxiliary variables are introduced.

$$\dot{y}_1 = -\varepsilon_1 y_1 + \psi_1 \left[\ddot{\xi}(\tau) + \left(\frac{1}{2} - a_h \right) \ddot{\alpha}(\tau) + \frac{T_{11}}{2\pi} \ddot{\beta}(\tau) + \dot{\alpha}(\tau) + \frac{T_{10}}{\pi} \dot{\beta}(\tau) \right] \quad (32)$$

$$\dot{y}_2 = -\varepsilon_2 y_2 + \psi_2 \left[\ddot{\xi}(\tau) + \left(\frac{1}{2} - a_h \right) \ddot{\alpha}(\tau) + \frac{T_{11}}{2\pi} \ddot{\beta}(\tau) + \dot{\alpha}(\tau) + \frac{T_{10}}{\pi} \dot{\beta}(\tau) \right] \quad (33)$$

The reformulated equations (21-27 and 28-33) could also be transformed into twelve first-order ODEs, and conveniently written in matrix form as

$$\dot{x}(t) = Ax + Bu + G \quad (34)$$

where $x = \{x_1, x_2, \dots, x_8, x_9, x_{10}, x_{11}, x_{12}\} = \{\alpha, \dot{\alpha}, \ddot{\alpha}, \xi, \dot{\xi}, \ddot{\xi}, \beta, \dot{\beta}, \ddot{\beta}, y_1, y_2, \sigma^A, \sigma^B, T^A, T^B\} \in \mathfrak{R}^{12}$, A and B are 12×12 matrices, and G is a vector containing all the nonlinear terms of the SMA actuator.

6. CONTROL LAW DESIGN AND NUMERICAL RESULTS

In this section, a flutter control law based on the state-dependent Riccati equation method, Tadi (2003) is designed. Consider the optimal infinite-horizon regulator problem, the performance index J is to be minimized subject to the system expressed by Eq. (34)

$$J = \int_0^{\infty} (x^T Q x + u^T R u) dt \quad (35)$$

where Q is a positive definite symmetric matrix and $R > 0$ for $x \in \mathfrak{R}^{12}$. In order to obtain the suboptimal solution of the preceding problem, we solve the state-dependent Riccati equation given by

$$A^T P + PA + Q - PBR^{-1}B^T P = 0 \quad (36)$$

for a symmetric positive definite matrix P, the feedback control law is given by

$$u = -R^{-1}B^T P x \quad (37)$$

Numerical simulation results are presented in this section. The values for the system parameters are taken from Tang, et. al. (2004) and the values for the Flexinol SMA wire are taken from Elahinia and Ahmadian (2005), and listed in table 1a and 1b, respectively.

6.1. Open loop system response

To study the effect of SMA actuator on the open-loop system response, the values of temperature of both actuator (A and B) are the same, that is, 20°C. Starting from the open-loop stability study of the aeroelastic system, the system response keeps stable until the velocity reaches $U=16$ m/s, with or without the SMA actuator presence. From Fig. 6, it can be observed that the SMA actuator system response needs less time to converge. In addition, the response amplitude is obviously smaller. Can be realized that the over time the amplitudes of motion for both cases decays. Note that the SMA actuator system to influence significantly the response of the system, making it the fastest. As the existence of SMA actuator, the stiffness of the connection between airfoil and control surface is increased. When the airfoil vibrates, the control surface is motivated through the SMA actuator connection. The higher connection stiffness will advance the control surface response.

Table 1: Physical parameters of the aeroelastic system

Parameter	Description	Unit	Value
l	Span	m	0.52
b	Semi-chord	m	0.127
a	Elastic axis	m	-0.0625
m_W	Mass of wing	kg	0.713
I_a	Mass moment of inertia	kg m ²	0.0185
I_b	Mass moment of inertia	kg m ²	0.000254
S_a	Airfoil static moment in pitch	kg m	0.0726
S_b	Airfoil static moment in flap	kg m	0.00395
K_a	Linear structural stiffness in pitch	N/m	42.8
K_h	Linear structural stiffness in plunge	N/m	2755.4
K_b	Linear structural stiffness in flap	N/m	3.3

Table 2: Flexinol SMA wire parameters and their value.

Parameter	Description	Unit	Value
m_{SMA}	SMA wire's mass	Kg	1.14×10^{-4}
A_R	SMA wire's circumferential area	m ²	4.712×10^{-4}
C_p	Specific heat of wire	kcal kg ⁻¹ °C ⁻¹	0.2
R_M	Resistivity (martensite)	Ω	76
R_A	Resistivity (austenite)	Ω	84
D_A	Austenite Young modulus	GPa	75
D_M	Martensite Young modulus	GPa	28
θ	SMA wire's thermal expansion factor	MPa °C ⁻¹	0.55
A_s	Austenite start temperature	°C	68
A_f	Austenite final temperature	°C	78
M_s	Martensite start temperature	°C	52
M_f	Martensite final temperature	°C	42

6.2. Closed-loop system response

The temperature-based controller is to minimize the vibration problem while positioning the SMA actuator at the desired angular position. The LQR control algorithm is used to calculate the applied current to the SMA wire. Applied current to the SMA wire is actual control input. This current is calculated based on the desired stress and the thermomechanical and heat transfer models of the SMA. For linearize the Eq. (34) we consider that the behavior of the SMA actuators are linear. For the SMA actuator A we assume that the SMA behavior correspond to linear stretch of the Fig. 1b. On the other hand, the actuator B is linearized assumed the linear behavior of SME effect with illustrate the Fig. 1a. In the following closed-loop situation, state coefficient matrix Q in performance index is chose as $Q = 10^{-11} I_{12 \times 12}$, and control input coefficient $R = 2 \times 10^{-4} \text{diag}([1 \ 1])$. The simulation was first performed with the flow velocity $U=15.0\text{m/s}$, which is above critical flutter speed. As shown in Fig. 7, after initial oscillatory transients the plunge and pitch states converge to zero. There is obvious difference between the SMA actuator system and non-SMA actuator system responses. The SMA actuator system response maximum amplitude is obviously smaller. The SMA actuator system states take less time to converge to zero after the transient oscillation, which behaves like a response of an over damping system. Figure 7d and 7e shows the system behavior as a function of time during the mode of temperature stabilization of both actuators considering $U=15.0\text{m/s}$. Figure 7f illustrates the control input applied to each actuator to stabilize the temperature at 20°C.

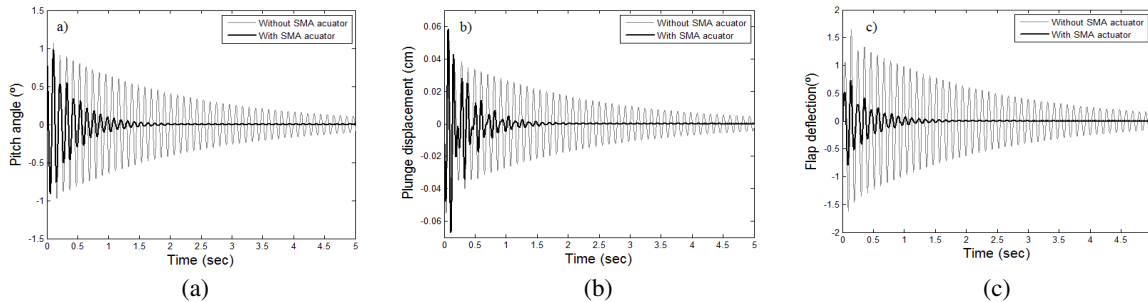
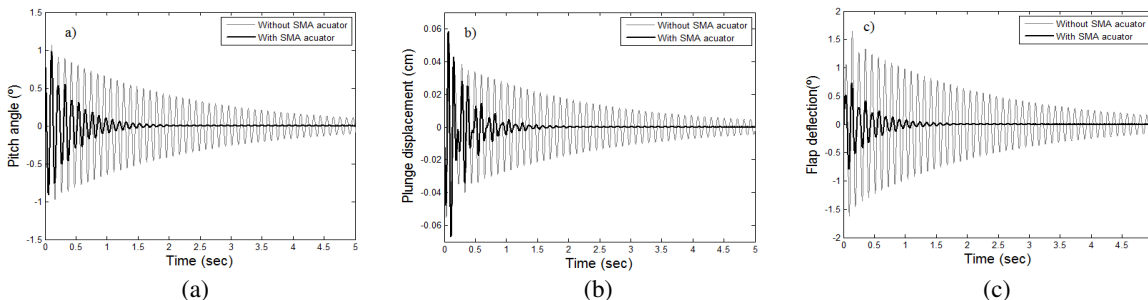


Fig. 6: Time histories of open-loop aeroelastic systems at $U=15.0\text{m/s}$: (a) pitch, (b) plunge and (c) flap



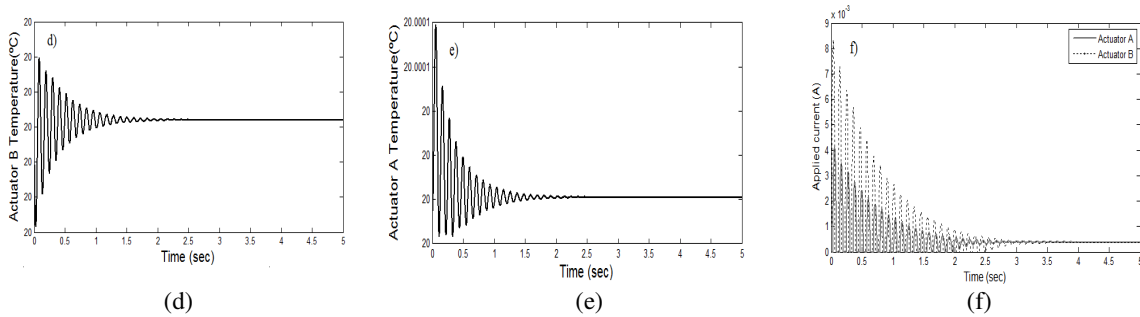


Fig. 7: Time histories of closed-loop aeroelastic systems at $U=15.0\text{m/s}$: (a) pitch, (b) plunge, (c) flap, (d) actuator A temperature, (e) actuator B temperature and (f) Applied electrical current in the actuators

Now we change the actuator B temperature according to Fig. 5a (step 1). The temperature of actuator A is constant and equal at room temperature, that is, 20°C . However, the actuator B temperature changes of 20°C to 90°C . The goal of this change is modified the camber of the wing. The camber is responsible for changing the flow around the airfoil and, consequently, is responsible for generating lift in a wing. The state coefficient matrix Q in performance index is chose as $Q=10^{-8} I_{12 \times 12}$, and control input coefficient $R=2 \times 10^{-5} \text{diag}([0.00581 \ 10000])$. Figure 8 shows the system response to the above control law. Note that by varying the temperature of the SMA actuator B the deflection of control surface features a flap angle of about 2.3° . When the flap going for down the equilibrium point of the system changed and this situation is show in Figs. 8a and 8b. Figure 8g shows the control input in actuators, realize that the electric current applied to the actuator B to keep it at the desired temperature is approximately 3.2A.

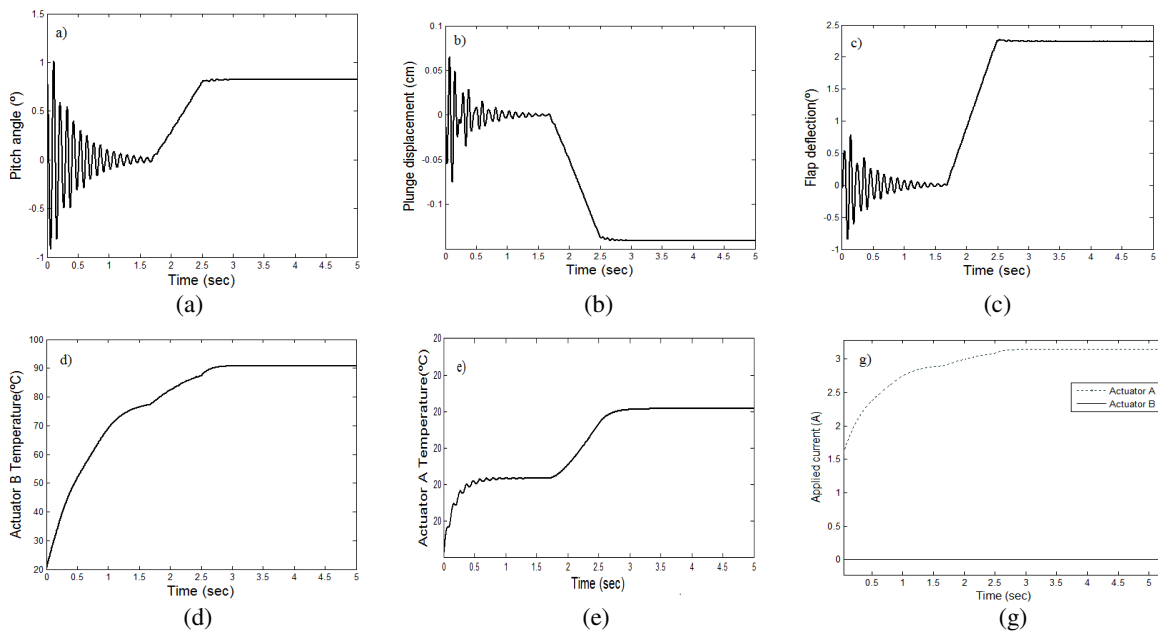


Fig. 8: Time histories of closed-loop aeroelastic systems at $U=15.0\text{m/s}$: (a) pitch, (b) plunge, (c) flap, (d) actuator A temperature, (e) actuator B temperature and (f) Applied electrical current in the actuators

7. CONCLUSION

This paper presents the design, testing and feedback control of a shape memory alloy (SMA) wire actuated wing flap. Based on the state space model of a three degrees-of-freedom airfoil section with SMA actuator, a suboptimal control law was designed by using the state-dependent Riccati equation method and applied for dynamic response suppression in this paper. The effects of control surface SMA actuator on the aeroelastic responses have been investigated. Because the nonlinear component in the control surface response amplitude decreases and becomes dominant, the effect of SMA actuator on the system response reduces the amplitude in all the degrees of freedom. In addition, the SMA actuator proposed shows some beneficial effect on the aeroelastic stability of the closed-loop system. This paper demonstrates the feasibility of using shape memory alloy actuators for wing flap movement control.

8. ACKNOWLEDGEMENTS

The authors thank the support of the Brazilian government Agency CNPq.

9. REFERENCES

- Alighanbari, H., 2002, "Stability and Bifurcations of an Airfoil-Aileron combination in Two-Dimensional Incompressible Inviscid Flow", 43rd AIAA/ASME/ASCE/AHS/ASC Structures, Structural Dynamics, and Materials Con. 22-25 April 2002, Denver, Colorado.
- Barker, J. M., and Balas, G. J., 2000, "Comparing Linear Parameter-Varying Gain-Scheduled Control Techniques for Active Flutter Suppression," *Journal of Guidance, Control and Dynamics*, Vol. 23, No. 5, pp. 948-955.
- Brinson, L. C., 1993, "One-Dimensional Constitutive Behavior of Shape Memory Alloys: Thermo mechanical Derivation with Non-Constant Material Functions and Refined Martensite Internal Variable", *Journal of Intelligent Material Systems and Structures*, Vol. 4, pp. 229-242.
- Dowell, E.H., Crawley, E.F., Curtiss Jr., Peters, D.A., H.C., Scanlan, R.H., Sisto, F., 2008, "A Modern Course in Aeroelasticity", Ed. Springer-Verlag, New York, USA, pp.746.
- Elahinia, M.H.; Ahmadian, M., 2005, "An enhanced SMA phenomenological model: II. The experimental study," *smart materials and structures*, Vol. 14, pp. 1309-1319.
- Guo, X., Lee, Y. Y., Mei, C., 2007, "Supersonic nonlinear panel flutter suppression using shape memory alloys", *Journal of Aircraft*, Vol. 44.
- Lin, C.M., Chin, W.L., 2006, "Adaptive decoupled fuzzy sliding-model control of a nonlinear aeroelastic system, *Journal of Guidance, Control, and Dynamics*, Vol. 29, pp. 206-209.
- Ibrahim, H. H., Tawfik, M., Negm, H. M., 2008, "Thermoacoustic random response of shape memory alloy hybrid composite plates", *Journal of Aircraft*, Vol. 45, No. 3.
- Mukhopadhyay, V., 2003, "Historical perspective on analysis and control of aeroelastic responses, *Journal of Guidance, Control, and Dynamics*, Vol. 26, pp. 673-684.
- Mavroidis, C., 2002, "Development of Advanced Actuator Using Shape Memory Alloys and Electrorheological Fluids", *Research for Non-Destructive Evaluation*, Vol. 14, pp. 1-32.
- Tadi,M., 2003, "State-dependent Riccati equation for control of aeroelastic flutter, *Journal of Guidance, Control, and Dynamics* Vol. 26, pp. 914-917.
- Tang, D., Henri, P.G., Dowell, E.H., 2004, "Study of Airfoil Gust Response Alleviation Using an Electro-Magnetic Dry Friction Damper. Part 1: Theory", *Journal of Sound and Vibration*, Vol. 269, pp. 853 - 874.
- Tawfik, M., Ro, J. J., Mei, C., 2002, "Thermal post-buckling and aeroelastic behavior of shape memory alloy reinforced plates", *Smart Materials and Structures*, Vol. 11, pp. 297-307.
- Williams, E.; Elahinia, M.H., 2008, "An Automotive SMA Mirror Actuator: Modeling, Design, and Experimental Evaluation", *Journal of Intelligent Material Systems and Structures*, Vol. 19, pp. 1425, 2008

8. RESPONSIBILITY NOTICE

The authors are the only responsible for the printed material included in this paper.

Appendix A. Theodorsen constants in Eqs. (21) - (28)

$$T_1 = -\frac{1}{3}\sqrt{1-c_\beta^2} (2+c_\beta^2) + c_\beta \cos^{-1} c_\beta, \quad T_2 = c_\beta (1-c_\beta^2) - \sqrt{1-c_\beta^2} (1+c_\beta^2) \cos^{-1} c_\beta + c_\beta (\cos^{-1} c_\beta)^2$$

$$T_3 = -\left(\frac{1}{8} + c_\beta^2\right) c_\beta^2 \cos^{-1} c_\beta + \frac{1}{4} c_\beta \sqrt{1-c_\beta^2} \cos^{-1} c_\beta (7+2c_\beta^2) - \frac{1}{8} (1-c_\beta^2) (5c_\beta^2 + 4)$$

$$T_4 = -\cos^{-1} c_\beta + c_\beta \sqrt{1-c_\beta^2}, \quad T_5 = -(1-c_\beta^2) - c_\beta^2 \cos^{-1} c_\beta^2 + 2c_\beta \sqrt{1-c_\beta^2} \cos^{-1} c_\beta, \quad T_6 = T_2$$

$$T_7 = -\left(\frac{1}{8} + c_\beta^2\right) \cos^{-1} c_\beta + \frac{1}{8} c_\beta \sqrt{1-c_\beta^2} (7+2c_\beta^2), \quad T_8 = -\frac{1}{3}\sqrt{1-c_\beta^2} (2c_\beta^2 + 1) + c_\beta \cos^{-1} c_\beta$$

$$T_9 = \frac{1}{2} \left[\frac{1}{3} \left(\sqrt{1-c_\beta^2} \right)^3 + a_h T_4 \right], \quad T_{10} = \sqrt{1-c_\beta^2} + \cos^{-1} c_\beta, \quad T_{11} = \cos^{-1} c_\beta (1-2c_\beta) + \sqrt{1-c_\beta^2} (2-c_\beta)$$

$$T_{12} = \sqrt{1-c_\beta^2} (2+c_\beta) - \cos^{-1} c_\beta (2c_\beta + 1), \quad T_{13} = \frac{1}{2} \left[-T_7 - (c_\beta - a_h) T_1 \right]$$